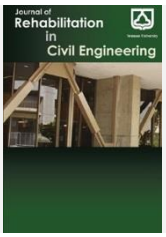

Journal of Rehabilitation in Civil Engineering

Journal homepage: https://civiljournal.semnan.ac.ir/

# Fire Behavior of Lightweight Reinforced Concrete Deep Beams and Enhanced Structural Performance via Varied Stirrup Spacing – An Integrated Study

**Ali Mohammad Ali [1]; Amir H Akhaveissy [1,*]; Bahaa Abbas [2]**

1. Department of Civil Engineering, Faculty Engineering, Razi University, Kermanshah, Iran
2. Department of Civil Engineering, Engineering Faculty, Kerbala University, Kerbala, Iraq
* Corresponding author: *ahakhaveissy@razi.ac.ir*

**ARTICLE INFO**

Article history:
Received: 11 August 2023
Revised: 08 October 2023
Accepted: 31 December 2023

Keywords:
Lightweight reinforced concrete;
Deep beams;
Fire condition;
Stirrup spacing;
Shear behavior;
Finite element method.

**ABSTRACT**

The behavior of lightweight reinforced concrete deep beams (LRCDBs) under fire conditions is investigated in this study, with a specific focus on the effect of varying transverse reinforcement spacing. Four LRCDB specimens with transverse reinforcement intervals of 60 mm and 150 mm are constructed and subjected to four-point bending tests at both normal and elevated temperatures. The ultimate load-bearing capacity of the specimens is increased by 6.9% when the spacing of transverse reinforcements is reduced from 150 mm to 60 mm. Additionally, the load-bearing capacity of the specimens with 60 mm and 150 mm stirrup spacing is reduced after exposure to fire, with reductions of 16.8% and 23.6% respectively. The ultimate deflection of the mid-span of the beam is also diminished by the heat from the fire. The analysis of the specimens is performed using Abaqus software and the Finite Element Method. The obtained results exhibit a strong agreement with the experimental data, providing valuable insights into the behavior of LRCDBs during fire conditions. These insights highlight the critical importance of designing appropriate transverse reinforcement.

E-ISSN: 2345-4423


**How to cite this article:**
Ali, A., Akhaveissy, A., & Abbas, B. (2024). Fire Behavior of Lightweight Reinforced Concrete Deep Beams and Enhanced Structural Performance via Varied Stirrup Spacing – An Integrated Study. Journal of Rehabilitation in Civil Engineering, 12(3), 132-151. https://doi.org/10.22075/jrce.2023.31484.1889

## 1. Introduction

Deep beams play a crucial role as structural components in a variety of structures, including high-rise buildings, bridges, silos, and power plants. As per the ACI 318-18 Standard [1], deep beams have a clear span length to height ratio of less than 4. Unlike slender beams, deep beams deviate from Bernoulli's principle, and the variations in strain along their height are not substantial. Instead, shear is the primary mode of failure [2–4] Consequently, the design of deep beams necessitates meticulous consideration of their shear behavior, especially in fire conditions, as it can significantly impact their structural response [5,6]. The analysis and design of reinforced concrete structures, particularly deep beams, are simplified by the strut and tie method (STM). Stresses are transferred using compressive struts and tensile ties. Since 2002, STM has been extensively utilized and is recommended by the ACI 318M-14 code. Experimental findings demonstrate that incorporating reinforcing struts and ties in continuous deep beams can reduce weight while preserving structural capacity [7–10].

The behavior of deep beams, which play a critical role as structural elements in various constructions, is significantly influenced by their design. The use of lightweight concrete in the construction of deep beams has gained significant popularity due to its advantageous qualities. These qualities include the reduction of weight and mass in structures, high porosity, low modulus of elasticity, and low thermal conductivity. These attributes make lightweight concrete an attractive option for improving structural fire resistance and enhancing resilience against lateral forces such as earthquakes [11]. Previous research has focused on investigating the impact of increasing beam depth on several parameters that affect deep beams, such as concrete compressive strength, reinforcement ratio, beam depth, shear span length-to-height ratio, and shear strength [12–16]. The studies indicate that an increase in beam depth leads to a reduction in shear strength, thereby suggesting the presence of a size effect [17,18]. According to Li et al. [19] findings, the height of reinforced concrete deep beams, without transverse reinforcements and with a shear span to height ratio of 0.89, has an impact on shear resistance. Increasing the beam height from 180 mm to 1440 mm results in a reduction in shear resistance of up to 32.3% and 27.3% for concretes with compressive strengths of 35 MPa and 50 MPa, respectively.

It has been shown by studies that the performance of both ordinary and deep beams can be significantly improved through the utilization of new materials and reinforcement techniques. For instance, replacing steel rebars with GFRP rebars in deep beams constructed from concrete with a compressive strength of 60 MPa leads to a 4% increase in bearing capacity and a 39% reduction in deformation [20]. Similarly, By increasing the ratio of transverse reinforcements in the tested samples from 0.47 to 0.84, the load in deep beams, reinforced with high-strength concrete (having a compressive strength of 172.9 MPa) and a shear span to height ratio of 0.79, is increased from 890 KN to 1060 KN [21]. In studies conducted by Ibrahim et al. [22], composite fiber polymers consisting of glass and carbon have been utilized to improve the behavior of deep beams. The samples reinforced with this polymer exhibit an increase in shear strength of up to 55.8% and an average increase in ultimate deflection of 62.1%. An increase in GFRP shear reinforcement ratio in concrete deep beams [23] results in a shift of the failure mode from shear compression to compression strut failure. The load-carrying capacity of the beams is increased by 35.5% and 73.5% at GFRP ratios of 0.32% and 0.47%,

respectively. However, the minimum recommended GFRP shear reinforcement in ACI 440.1R-15 is found to be ineffective in enhancing shear capacity and controlling shear cracks in the tested GFRP-RC continuous deep beams. The shear strengthening of lightweight self-consolidating concrete (LWSCC) beams, reinforced with GFRP bars, is examined by Nawaz et al. [24]. It is revealed that FRP design standards overestimate shear capacity, thus requiring the use of a modified equation. The shear capacity of LWSCC beams is increased by 33.3% to 168% through the incorporation of longitudinal reinforcement and horizontal strips. Furthermore, investigations have been conducted on the application of lightweight concrete in deep beams, and research suggests that it can decrease the weight of the structure while maintaining satisfactory shear and failure behavior [25]. Conversely, the introduction of steel fibers into lightweight concrete has been observed to enhance the ultimate load-bearing capacity of the beams. The inclusion of just one percent of steel fibers in the specimens led to an average increase of 23% in the ultimate load-bearing capacity [26].

The behavior of deep beams under fire conditions has been the subject of study. The effects of fire on beams constructed using lightweight and normal concrete are investigated in one particular study. As the temperature increases to 750°, a reduction of 21.3% in load capacity is experienced for normal concrete, and a reduction of 37% is experienced for lightweight concrete. At 750°, the residual strength is measured at 78% for lightweight concrete and 63% for normal concrete [27]. The deflection of the beam is observed to increase as the fire exposure time and load increase. Conversely, an increase in the distance between supports leads to a decrease in deflection [28]. In addition, the influence of different aggregates on the shear performance of reinforced concrete deep beams at elevated temperatures is investigated in the study. The findings reveal that increasing the temperature from 25 to 600 °C leads to a 23.1% decrease in shear strength for samples with limestone aggregates and a 40.5% decrease for samples with quartz aggregates. Moreover, the temperature rise causes a 34% decrease in initial stiffness for limestone aggregates and an 80% decrease for quartz aggregates. Limestone aggregates, weighing 1575 kg/m$^3$, exhibit superior performance in terms of thermal intensification compared to quartz aggregates, weighing 1487 kg/m3 [29].

The behavior of reinforced concrete deep beams and ordinary beams with fiber or high-strength concrete under different loading and environmental conditions has been extensively investigated in previous research [2–4,6,12,13,16–18,30]. Extensive research has been conducted on the effects of heat on these beams [9,20–22,31–33]. However, there is a notable gap in the literature regarding the behavior of reinforced concrete deep beams with lightweight concrete when subjected to fire. Elevated temperatures in fire conditions result in the loss of strength and stiffness of concrete, ultimately leading to structural failure [5,14,15,19]. Therefore, comprehending the behavior of reinforced concrete deep beams with lightweight concrete when exposed to fire is essential for the design of safe and efficient structures in fire-prone environments [27,29,34,35]. The aim of this study is to examine the impact of shear reinforcement distance on the residual strength of deep beams constructed with lightweight concrete, both before and after exposure to fire conditions. The study aims to provide valuable insights into the behavior of these beams under fire conditions and contribute to the formulation of design guidelines for reinforced concrete deep beams with lightweight concrete in environments prone to fire hazards.

## 2. Experimental Program

### 2.1. Details of experimental specimens

Table 1 presents the geometric characteristics and details of the experimental specimens, while Figure 1 illustrates the geometry of the specimens. Simple supports, positioned with a distance of 200 mm from the center of the supports to the end of the beam, and a spacing of 1000 mm between supports, are utilized in the tests. The specimens possess uniform dimensions, with a net length of 1400 mm, a height of 450 mm, and a width of 100 mm. The concrete cover size at the top and bottom of the cross-section remains consistent across all experimental specimens, measuring 20 mm.

**Table 1.** Reinforcement Specifications and Cross-Sectional Dimensions.

| Beam Specimen | Reinforcement | | Traversal Bars | Fire Condition |
|---|---|---|---|---|
| | **Top** | **Bottom** | | |
| DBS6W | 2Φ10 | 2Φ16 | Φ10@60 | No |
| DBS6F | 2Φ10 | 2Φ16 | Φ10@60 | Yes |
| DBS15W | 2Φ10 | 2Φ16 | Φ10@150 | No |
| DBS15F | 2Φ10 | 2Φ16 | Φ10@150 | Yes |

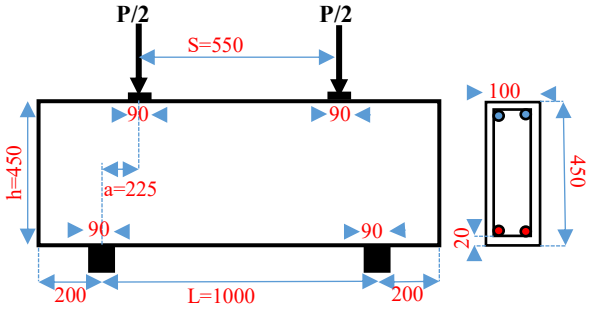


**Fig. 1.** Geometric characteristics of lightweight RC deep beam experimental specimens (all sizes are in mm).

According to Table 1, the deep beam experimental specimens are constructed using steel bars with diameters of 10 mm and 16 mm. The longitudinal tension and compression reinforcements are utilized, with the 16 mm and 10 mm diameter bars being employed, respectively. The transverse reinforcements are comprised of 10 mm diameter bars, which are positioned at intervals of 60 mm and 150 mm between each reinforcement.

### 2.2. Material properties

The construction of the LRCDB experimental specimens typically involves the use of lightweight concrete and steel reinforcement. The lightweight concrete is produced by utilizing lightweight expanded clay aggregates (LECA) manufactured by Kashan Factory, Iran, and fine aggregates obtained from a mine in the vicinity of Karbala city, Iraq. The size distribution of the grains is determined through granulation testing, following the ASTM-C136 [36] standard, as depicted in Figure 2. Lightweight concrete production employs Type-2 cement from Opc factory, Iraq, along with a super plasticizer added at a dosage of 1% relative to the weight of cement. A mixed design is employed after the granulated aggregates are prepared, and several trials and errors are conducted, as outlined in Table 2. The quantities of each material required to prepare one cubic meter of lightweight concrete are specified in the table. Cylindrical specimens are fabricated according to the criteria outlined in the ASTM standard, and their cylindrical compressive and tensile strengths are assessed based on ASTM-C39 [37] and ASTM-C496 [38] respectively.

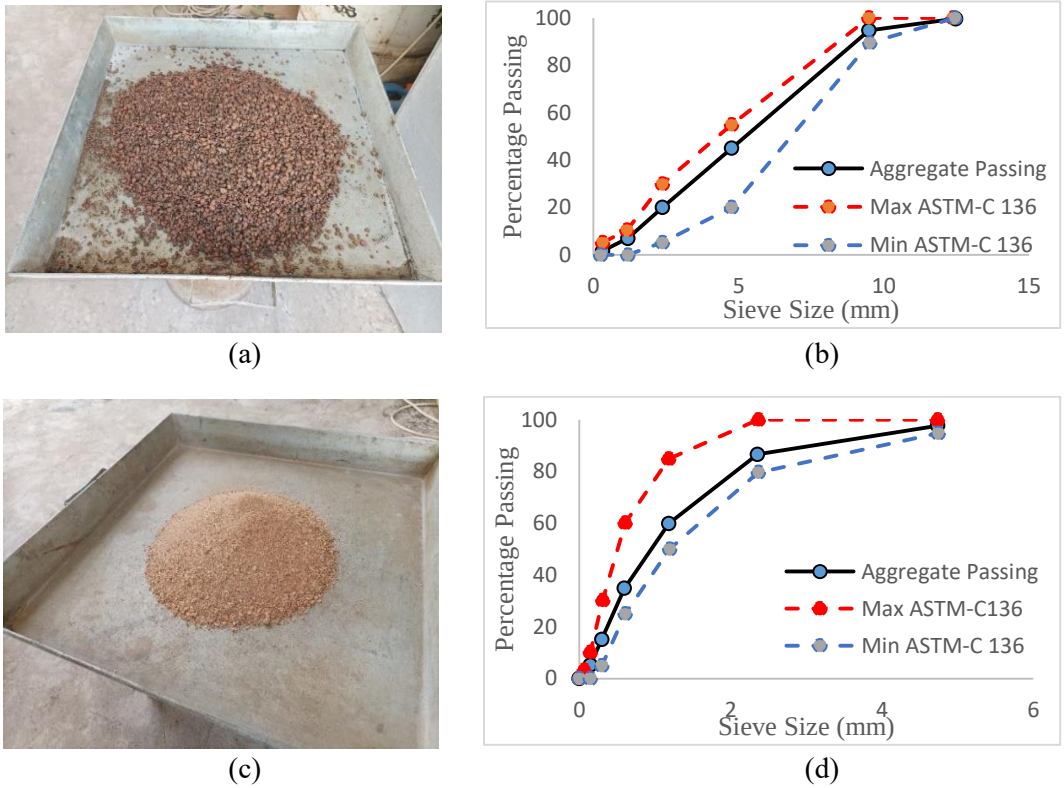


**Fig. 2.** (a) Lightweight expanded clay aggregate (LECA) (b) Gradation curve of course Aggregate (LECA) (c) fine aggregates (d) Gradation curve of fine aggregates (sand).

**Table 2.** Lightweight concrete mixing design for one cubic meter of concrete.

| Material | Cement (kg) | W/C | Course Agg.(LECA) (kg) | Fine Agg. (sand) (kg) | Superplasticizer (kg) |
|---|---|---|---|---|---|
| Proportion (kg/m3) | 510 | 0.41 | 475 | 625 | 5.4 |

The cylindrical compressive and tensile strengths of the concrete, both before and after exposure to fire conditions, are presented in Table 3. The mechanical properties of the steel reinforcement, manufactured by Arcelor Mittal factory, Ukraine, are presented in Table 4.

**Table 3.** cylindrical compressive and tensile strengths of concrete samples before and after fire conditions.

| Specimen | Density (kgf/m$^3$) | Avg (kgf/m$^3$) | Compressive Strength (MPa) | Avg (MPa) | Tensile Strength (MPa) | Avg (MPa) | fire condition |
|---|---|---|---|---|---|---|---|
| S01 | 1766 | | 37.2 | | 2.65 | | No |
| S02 | 1803 | 1773.33 | 38.24 | 37.81 | 2.84 | 2.78 | No |
| S03 | 1751 | | 38 | | 2.86 | | No |
| S04 | 1711 | | 25.5 | | 1.36 | | Yes |
| S05 | 1737 | 1723.67 | 26.1 | 25.33 | 1.6 | 1.48 | Yes |
| S06 | 1723 | | 24.4 | | 1.49 | | Yes |

**Table 4.** Mechanical Properties of Stirrups and Longitudinal Steel Bars for Reinforced Concrete Deep Beams.

| Yield strength (MPa) | Tensile strength (MPa) | Maximum tensile strain (%) | Elastic modulus (GPa) |
|---|---|---|---|
| 540 | 673 | 21 | 212 |

## 2.3. Preparation of experimental specimens

This study includes the preparation and testing of four samples of LRCDB. The preparation of the deep beam experimental specimens for testing comprises four steps: (1) concrete production, (2) reinforcement, (3) concrete placement, and (4) placement of the specimens in the furnace. The reinforcement of the specimens is illustrated in Figure 3.

**Fig. 3.** Reinforcement, formwork, concreting of experimental specimens.

## 2.4. Fire exposure

The effect of fire on reinforced concrete deep beams is investigated through an experimental procedure. The specimens are subjected to thermal loading in a furnace. The procedure begins with the construction of the specimens, including the DBS15F sample with a transverse reinforcement spacing of 150 mm and the DBS6F sample. Subsequently, the specimens are placed inside a metal furnace, and heat is applied to one side to simulate the effect of fire, as depicted in Figures 4(b) and 4(c). Flames are ignited beneath the specimens at eight points, with a distance of 200 mm between them. Thermal loading is conducted following the standard fire protocol used in previous studies, utilizing the time-temperature diagram outlined in ASTM-E119 [39]. The Time-temperature diagram of external fire, according to ASTM-E119 [39] and the observed experimental data, is shown in Figure 5. The rate of heat increase during thermal loading is measured using a thermocouple, which is installed in the middle and underneath the beam, as illustrated in Figure 4(b). The time-temperature diagram employed in the experimental specimens closely adheres to the ASTM-E119 standard. Once the furnace temperature reaches the desired level, the furnace is turned off, and the specimens are transferred to an exterior room to cool gradually. Following the completion of the fire exposure and cooling process, the specimens are subjected to a bending load. The furnace details are presented in Figure 4(a). The experimental procedure provides valuable insights into the behavior of reinforced concrete deep beams under fire conditions, offering essential information for the design of safe and reliable structures in fire-prone environments.


(a)

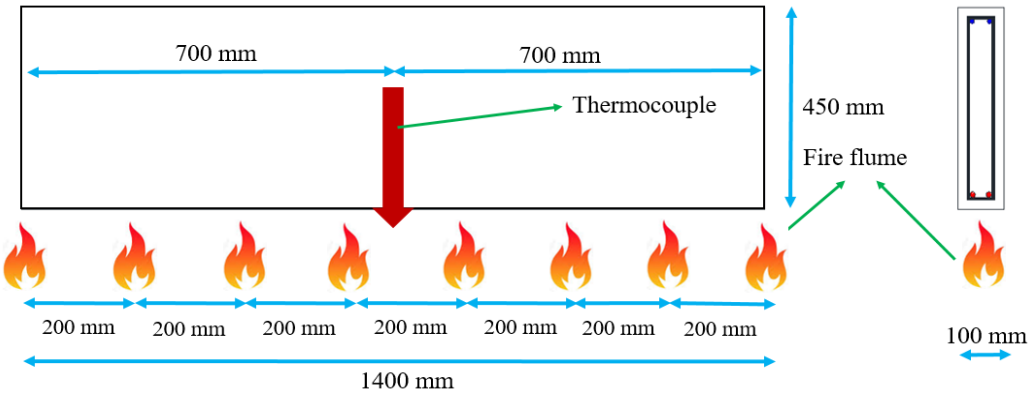


(b) (c)

**Fig. 4.** (a) Details of Furnace Used for Thermal Loading of Reinforced Concrete Specimens(b)Experimental Investigation of Deep Beam Behavior Under Thermal and Load Conditions (c) Sectional Analysis of Deep Beams Reinforced with Steel and GFRP Rebars.

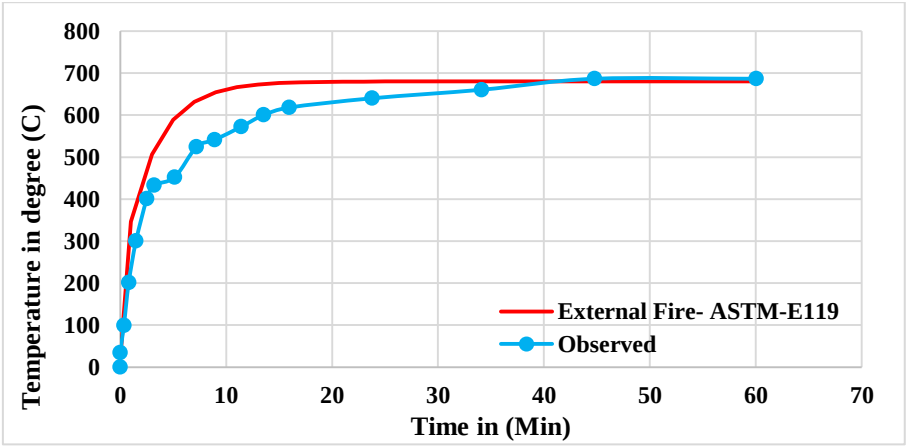


**Fig. 5.** Time-temperature diagram of external fire according to ASTM-E119 [39] and experimental observed.

## 2.5. Test setup

In the first step of the experimental setup, a hydraulic jack is installed to apply the load to the specimens. The load quantity is measured using a load cell (spoke type DYLF-102 high precision weighing) after connecting an LVDT (Miniature spring automatic reset electronic ruler KTR displacement sensor) and strain gauges to a data logger (NI PCI-6251 M-Series multifunction DAQ). The load cell, LVDT, and strain gauges are utilized to measure the response of the specimens to the applied load and provide data on the structural behavior of the LRCDBs under load. The data logger records and stores the data obtained

from the load cell, LVDT, and strain gauges. The experimental setup allows for the investigation of the load-carrying capacity and structural behavior of LRCDBs, which can contribute to the design of lightweight and efficient structures.

The specimens of lightweight reinforced concrete deep beams (LRCDBs) are subjected to concentric and static loading at two points using a 100-ton hydraulic jack in the structural laboratory of Karbala University. In four-point bending tests on concrete deep beams, a constant loading speed of 1 mm/s is utilized to simulate static loading. This speed is also employed to monitor the propagation of crack tips and prevent sudden catastrophic failure [40]. This controlled loading rate ensures safety, accurate data acquisition, and compliance with testing standards. Simple support conditions are employed for all experimental specimens on both sides, with 10 mm thick, 90 mm long and 100 mm wide steel plates used under the hydraulic jack head and support to prevent damage to the LRCDB specimens. An I-shaped steel section is utilized to transfer the applied load to the deep beams of the jack. The vertical load from the hydraulic jack is transferred as a two-point load to the LRCDB through the I-shaped section steel beams. The displacement of the mid-beam is measured using one LVDT, and another LVDT is placed at one-third of the span. The loading conditions of the test setup are illustrated in Figure 6. The experimental setup and loading conditions provide insights into the load-carrying capacity and structural behavior of LRCDBs under concentric and static loading, which are essential for designing lightweight and efficient structures.

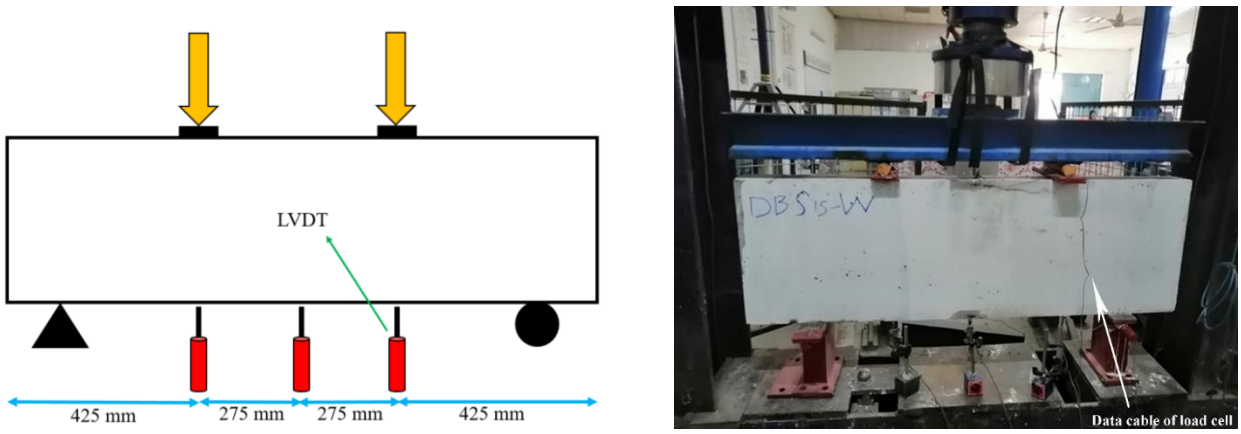


**Fig. 6.** Experimental Setup for Load Testing of Lightweight Reinforced Concrete Deep Beams.

## 3. Test results and discussion

### 3.1. Load–deflection Curves

The load-deflection curves of the mid-span of the LRCDB experimental specimens are depicted in Figure 7. Based on Figure 7, the shear and flexural capacities of the pre-fire experimental specimens increase when the distance between the shear reinforcements is reduced from 150 to 60 mm, without significantly affecting stiffness. On the other hand, in the post-fire test samples, increasing the distance between the shear reinforcements leads to a decrease in bending and shear capacity and stiffness. Fire causes substantial alterations in the behavior of LRCDB, leading to concrete damage and diminished capacities in stiffness, bending and shear. Moreover, as shown in Figure 7, the drop in strength is lower in the fire-exposed specimens, possibly due to concrete damage and the failure of longitudinal reinforcements to reach yielding.

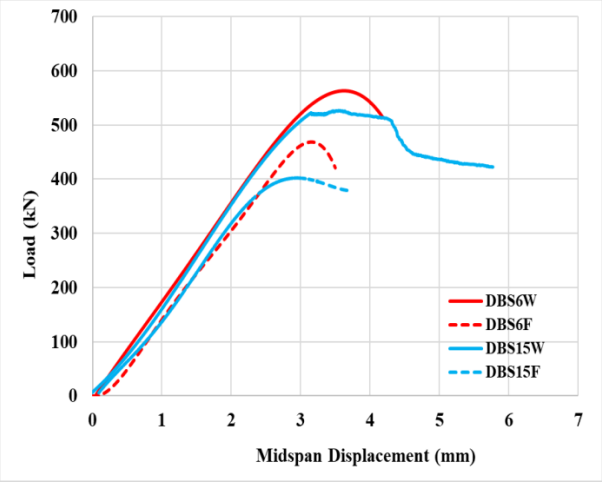


**Fig. 7.** Load – mid-span Displacement for experimental specimens.

## 3.2. Ultimate load and cracking load

The cracking load and ultimate load of the lightweight RC deep beam experimental specimens are provided in Table 5. Based on the results in Table 5, reducing the distance between the shear reinforcements from 150 mm to 60 mm increases the cracking load by 6.8% and 14.5% in the pre-fire and post-fire experimental specimens, respectively. This reduction in distance has a positive effect on the cracking load bearing capacity of the experimental specimens, both before and after fire. Fire reduces the cracking load by 53.3% and 50% in the specimens with 150 mm and 60 mm transverse reinforcement spacing, respectively. The cracking load represents the load at which the first visible crack appears on the beam's surface. It is the point at which the tensile stress exceeds the concrete's tensile strength, resulting in crack formation. Additionally, reducing the distance between the shear reinforcements before the fire condition increases the ultimate load by 6.9%, and this effect is even more pronounced after the fire condition (16.5%). Furthermore, in the fire condition, the ultimate load decreases by 23.6% and 16.8% in the test samples with a transverse reinforcement spacing of 150 mm and 60 mm, respectively.

**Table 5.** Comparison of the experimental loads with ACI [1] code and Theory [2].

| Specimen | Experimental Cracking Load (KN) | Experimental ultimate load (KN) | ultimate load from **ACI** (KN) | Ultimate load from **Kong theory** (KN) |
|---|---|---|---|---|
| DBS15W | 150.2 | 526.75 | 579.8 | 734.93 |
| DBS15F | 70.12 | 402.16 | - | - |
| DBS6W | 160.5 | 563.05 | 783.32 | 734.93 |
| DBS6F | 80.3 | 468.50 | - | - |

The shear resistance of a reinforced concrete beam can be attributed to four main factors: tensile longitudinal bars, compressive zone concrete, interlocking of aggregates, and transverse reinforcements. In the case of lightweight reinforced concrete deep beams, the effect of these factors on shear resistance can vary. The experimental results show a difference in capacity of about 6.9% between DBS15W and DBS6W. It is observed that in lightweight concrete, the contribution of interlocking of aggregates and compressive zone concrete to shear resistance is more significant than the reduction in distance between shear reinforcements. This is likely due to the reduced weight and increased porosity of the lightweight aggregates, which can impact the interlocking of aggregates and the compressive zone concrete. Additionally, lightweight aggregates have a lower modulus of elasticity, resulting in less resistance of lightweight concrete against concentrated loads. The analysis of factors affecting shear resistance in lightweight reinforced concrete deep beams emphasizes the importance of considering the properties of lightweight aggregates and their impact on the interlocking of aggregates and compressive zone concrete during the design of structures with lightweight concrete.

Table 5 also presents the ultimate load of the experimental specimens according to the ACI 318-18 [1] standard and the theory proposed by Kong [2]. However, based on previous studies [41–43] the ultimate load calculated based on ACI versus the ultimate load of the laboratory samples is conservative, that is not considered in this case. Kong's Eq. 1 is utilized to determine the ultimate shear strength of the deep beam, which considers the contribution of the concrete ($P_c$), tensile reinforcements ($P_s$), and web reinforcement ($P_w$).

$$Q_u (= P_u / 2) = P_c + P_s + P_w \quad (1)$$

$$P_c = \frac{cbD}{\sin(\beta)\cos(\beta)(\tan(\beta)+\tan(\phi))}$$

$$P_s = F_s \left[ \frac{\tan(\beta)\tan(\phi)-1}{\tan(\beta)+\tan(\phi)} \right]$$

$$c = \frac{\sqrt{f_c' f_t'}}{2} \qquad \tan\phi = \frac{(f_c' - f_t')}{2\sqrt{f_c' f_t'}}$$

In Kong's Eq. 1 for determining the ultimate shear strength of a deep beam, $F_s = A_s f_{sy}$; $f_{sy}$ represents the yield point stress of the tensile steel, $\beta$ is the angle of inclination of the rupture plane with respect to the horizontal, b is the width of the beam, D is the depth of the beam, $f_c'$ and $f_t'$ and are the compressive and tensile strengths of the concrete, respectively. Notably, web reinforcement is not utilized in the examined deep beams in this study. Based on the cross-sectional dimensions of the beam shown in Figure 1 and the compressive and tensile strengths of the concrete (37.81 and 2.78, respectively), the ultimate load capacity, as determined by Eq. 1, is 734.93 KN ($P_c = 333.03, P_s = 401.9$). However, the experimental ultimate load of the samples is lower than the ultimate load calculated using the ACI method and Eq. 1. This discrepancy may be due to the weaker interlocking of lightweight concrete aggregates, which suggests that these equations should be modified for lightweight concrete. Figure 8 illustrates a schematic image of the deep beam under two-point loading with reinforcements and a failure plane.

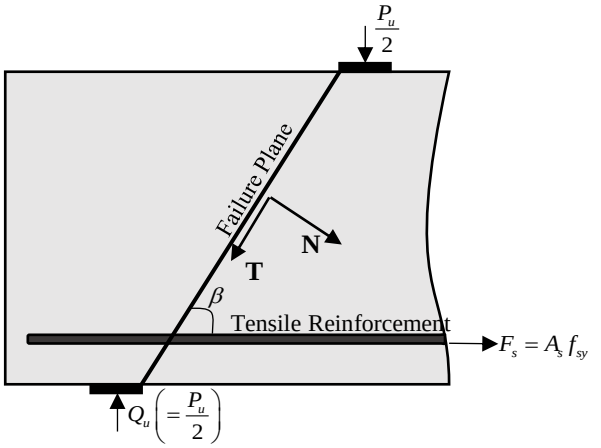


**Fig. 8.** Typical RC deep beams ultimate strength under two-point loading.

## 3.3. Deformation (deflection)

Table 6 presents the deflection amounts of the samples at the moment of cracking and ultimate deflection. The results show that in the samples with a stirrup distance of 150 mm, the fire-induced heat reduces the ultimate deflection of the middle of the beam span by 17.3%, while this reduction is 12.9% for the samples with a stirrup distance of 60 mm. Moreover, reducing the stirrup spacing from 150 mm to 60 mm at normal temperature and after fire increases the ultimate deflection of the middle of the beam span by 1.7% and 7.1%, respectively. These findings indicate that fire reduces the deflection and causes the samples to exhibit a more brittle fracture, which is consistent with the results reported in other studies [27,44].

**Table 6**. Mid-span deflection of specimens.

| Specimen | Cracking deflection $\delta_c$ (mm) | Ultimate deflection $\delta_u$ (mm) |
|---|---|---|
| DBS15W | 0.94 | 3.57 |
| DBS15F | 0.60 | 2.95 |
| DBS6W | 0.91 | 3.63 |
| DBS6F | 0.64 | 3.16 |

### 3.4. Cracking pattern and failure modes

Figure 9 illustrates the cracking of the experimental specimens. In Figure 9(a), the first hairline crack in the DBS6W specimen is observed at the support area as the load reaches 160 KN. Subsequently, cracks form in the tensile part of the cross-section and middle of the DBS6W as the load is increased to 230 KN. Further increase in the load leads to the growth and expansion of the crack toward the support, making the DBS6W specimen susceptible to shear failure mode. Figure 9(b) shows that hairline cracks are formed in the middle of the DBS6F specimen and adjacent to the support as the load reaches 80 KN. As the load approaches 140 KN, these hairline cracks grow and expand around the support. As the load is increased to 260 KN, cracks grow and expand toward the compression portion of the section. Oblique cracks are formed close to the support at 300, 320, and 337 KN loads, and the DBS6F specimen undergoes flexural-shear failure mode. Figure 9(c) reveals that hairline cracks are formed in the middle of the DBS15W specimen as the load reaches 150 KN. simultaneously, some cracks are observed near the support area diagonally. As the load increases, the gaps tend to expand around the support and middle areas of the specimen, and the DBS15W specimen undergoes shear failure mode. Finally, in Figure 9(d), hairline cracks are initially formed in the compressive part of the cross-section, middle of the beam span, and near the support when the load is 70 KN. As the load is increased, these cracks grow and expand obliquely around the support area, and the DBS15F specimen undergoes shear failure mode.

Analysis of Figure 9 suggests that a positive effect on crack width in the specimens prior to the fire is observed when the distance between shear reinforcements is reduced. Specifically, increasing the distance of shear reinforcements from 60 to 150 mm results in a reduction in the cracking load. However, a comparison of the specimens tested before and after the fire reveals that the fire has an adverse effect on crack width, likely attributable to concrete spalling and fire damage.

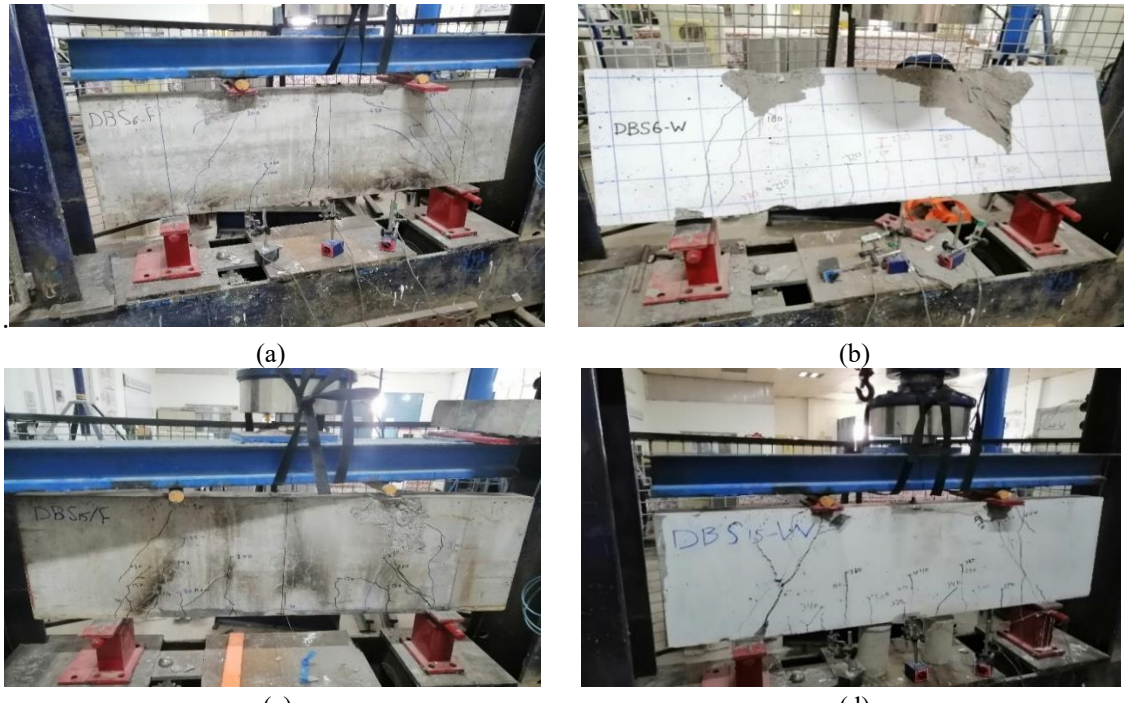


(a) (b)

(c) (d)

**Fig. 9.** Cracking pattern of experimental specimens at the moment of failure in (a) DBS6W (b) DBS6F (c) DBS15W (d) DBS15F.

Based on Figure 10, local damage occurs in all samples due to the effect of compressive stress concentration in the loading areas or supports. In the case of the DBS6F sample, which has a stirrup distance of 60mm and is exposed to fire, cracks formed in the middle of the beam expand almost to the entire height of the beam, indicating that the entire bending capacity of the concrete section is utilized. However, in the other samples, the bending cracks rise only up to the middle of the height of the beam, and the beam undergoes shear failure before the section reaches its bending capacity.

The analysis of the effect of fire on lightweight reinforced concrete deep beams is based on the observation of damage and spalling phenomenon in the experimental specimens. As observed in Figure 9, the samples exposed to fire show slight damage, and the phenomenon of concrete surface spalling is not significant. This can be attributed to the presence of porosity in lightweight concrete, allowing water vapor to escape without causing damage or flaking of the concrete surface. The experimental results indicate that lightweight concrete demonstrates acceptable fire resistance, which is an important consideration in the design of structures for fire-prone environments. The analysis of the damage and spalling phenomenon in lightweight reinforced concrete deep beams provides valuable insights into the behavior of lightweight concrete under fire conditions and can contribute to the development of safer and more resilient structures.

## 4. Numerical modeling

In deep beams, the height-to-span ratio is high, and strain distribution is non-linear, leading to rampant shear behavior. Therefore, numerical studies are necessary in addition to experimental investigations, and finite element modeling is critical in structural engineering.

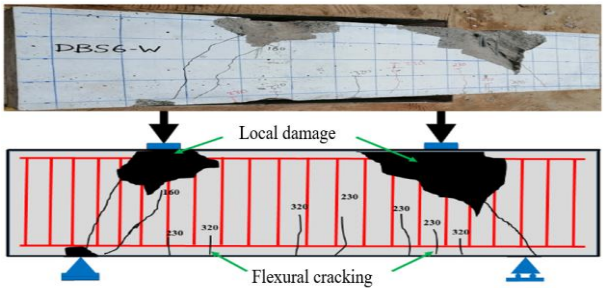

(a) DBS6W

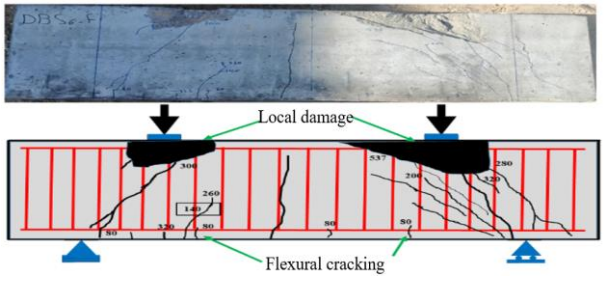

(b) DBS6F

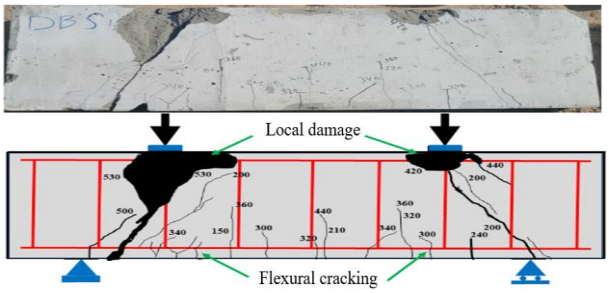

(c) DBS15W

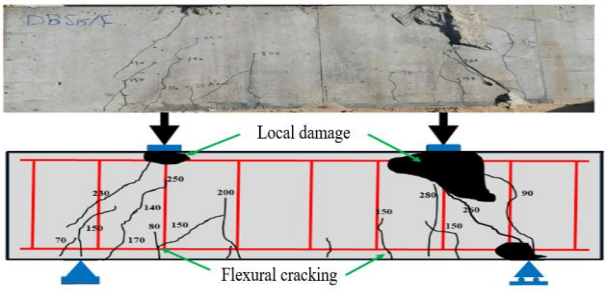

(d) DBS15F

**Fig. 10.** Experimental results of failure modes and cracking a) DBS6W b)DBS6F c) DBS15W d)DBS15F.

This research aims to precisely identify and examine the behavior of the experimental specimens using numerical modeling. The DBSW15 and DBS15F experimental specimens are modeled using FEM, and the results obtained from the numerical models and experimental specimens are compared and discussed. The numerical model of the

experimental specimens is first drawn in a 2-D environment and then transferred to a 3-D environment. The steel and concrete sections are considered solid and deformable. The concrete damage plasticity model defines concrete materials [45,46], and the failure criterion controls the uniaxial stress and tensile response. The Hognestad model [47] is used for the uniaxial response of concrete to pressure in this study. The behavior of lightweight reinforced concrete deep beams is modeled by analyzing the uniaxial compressive and tensile behavior of the concrete and steel. Figures 11(a) and 11(b) show the stress-strain diagram for the uniaxial compressive and tensile behavior of the concrete, respectively. Although these curves are typically used for normal strength concrete, in this research, they are applied to model the behavior of structural lightweight concrete, as the compressive strength of the specimens is around 37.8 Mpa. The behavior of the steel is assumed to be known, and slip between the steel rebar and concrete is neglected, as in previous research studies [12,14,48]. Figure 11(c) indicates that a two-line model is used to simulate the compressive and tensile behavior of the steel rebars. In the conditions before the fire, the elasticity coefficient of the rebars is found to be 2.1e5, and the Poisson's coefficient for the rebars is considered to be 0.3.

The material behavior modeling of lightweight reinforced concrete deep beams provides valuable insights into the structural behavior of these beams and can aid in the design of lightweight and efficient structures.

The displacement control model of deep beams is simulated using nonlinear static analysis. Additionally, the interaction between rebars and concrete is constrained in the embedded region. A 4-node linear tetrahedron mesh with a size of 50 mm is utilized for steel rebar, while a mesh with the same topology but a size of 25 is chosen for concrete. Figure 12 illustrates the reinforcement details, geometric characteristics, numerical model boundary conditions, and numerical model meshing.

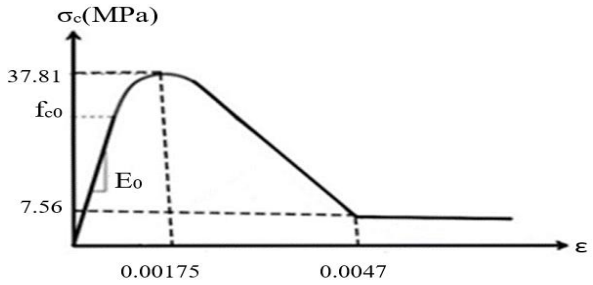


(a) Uniaxial response of concrete to pressure.

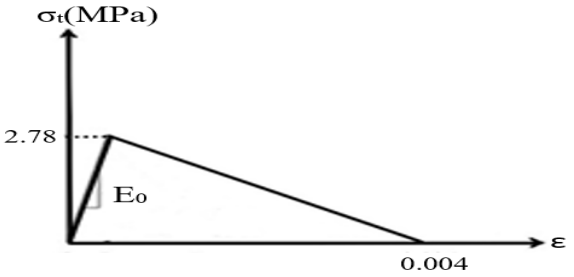


(b) Uniaxial response of concrete to tensile.

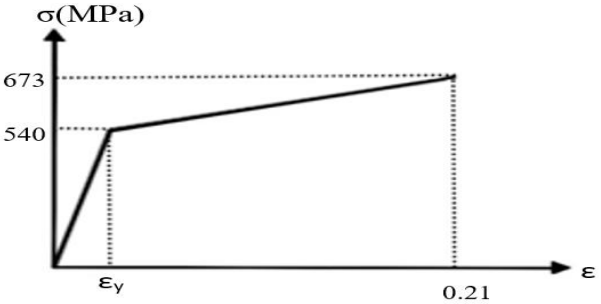


(c) Ideal stress-strain diagram of steel with hardening

**Fig. 11.** a) Uniaxial response of concrete to pressure b) Uniaxial response of concrete to tensile c) Ideal stress-strain diagram of steel with hardening.

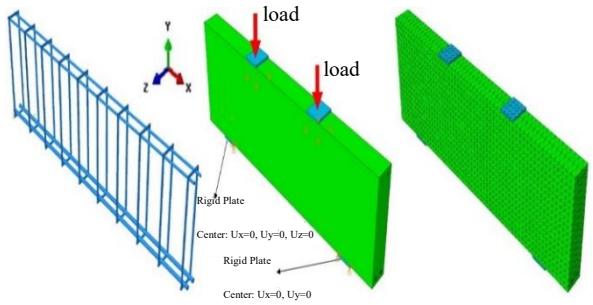


(a) (b) (c)

**Fig. 12.** Numerical model a) Reinforcement details b) Boundary conditions of numerical model c) Mesh.

### 4.1. Load-displacement and ultimate load of numerical models

The load-displacement diagram of the numerical models and experimental specimens is represented by Figure 13. The initial stiffness of numerical models for lightweight reinforced concrete deep beams is compared to that of experimental specimens when displacement is applied. It is found that the initial stiffness of the numerical models is higher than that of the experimental specimens. This discrepancy can be attributed to simplifications made during modeling or errors that commonly occur during experiments. The numerical models may not fully capture all the complexities and uncertainties associated with the behavior of real-world structures. Additionally, errors can occur during experiments due to various reasons, such as equipment limitations, data collection, and analysis methods. The comparison of initial stiffness between numerical models and experimental specimens emphasizes the importance of validating numerical models with experimental data and considering the uncertainties associated with both modeling and experimental methods. This contributes to the development of more accurate and reliable models for predicting the behavior of lightweight reinforced concrete deep beams under different loading and environmental conditions.

The slope of the numerical model diagram becomes approximately equal to that of the experimental specimen diagram as the displacement increases. Although the point-related displacements at ultimate load differ slightly between the numerical models and experimental specimens, the numerical models successfully predict the ultimate load. In the case of experimental specimen DBS15W, the ultimate load is 526.75 KN, while the predicted value in the numerical model has a 6% difference at 497.09 KN. For experimental specimen DBS15F, the ultimate load is 402.16 KN, while the predicted value in the numerical model has a 5.1% difference at 382.79 KN. After reaching the ultimate load, a drop in resistance due to specimen failure is observed in both the numerical models and experimental specimens of DBS15W and DBS15F. Based on Figure 13, there is a good consistency between the numerical outputs and experimental results.

As shown in Figure 13, the force from loading is absorbed by the concrete until point (a). At point (a), the concrete tensile stress reaches the modulus of rupture, causing cracking in the tensile area, and the curve drops to point (b). From point (b) to point (c), only the tensile reinforcements are able to withstand the tensile force. From point (c) to point (d), the behavior of the concrete becomes nonlinear in the compressive zone. The beam resistance value approaches the ultimate load at point (d). After point (d), the beam curvature significantly increases due to the yielding of the rebar until rupture occurs at point (e).

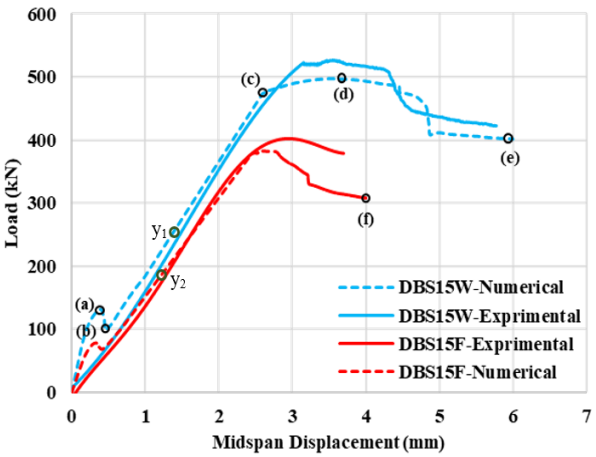


**Fig. 13.** Comparison of load-displacement diagrams between numerical models and experimental specimens.

In the examined models of samples DBS15W and DBS15F, the tensile reinforcements start to yield when the loading reaches 259.93 and 192.31 KN, respectively. These points are indicated in Figure 13 as y1 and y2. Therefore, in the samples exposed to fire, the load-

bearing capacity of the concrete weakens due to spalling and loss of tensile strength.

## 4.2. Failure mode of the numerical models

Figure 14 displays the PEEQ contour of the numerical models, revealing the cracking pattern and failure mode. In the DBS15W numerical model, cracking initiates in the shear area of LRCDB and then expands to the mid-span tensile zone of the deep beam. The failure in the DBS15W numerical model is of shear type, similar to the experimental specimen. In DBS15F, cracks begin to grow in the shear zone and the area close to the support, and then expand to the deep beam's tensile region. However, compared to DBS15W, a larger part of the deep beam's tensile area is damaged in the DBS15F model. This is because the concrete's tensile strength is reduced when exposed to fire. Furthermore, since fire exposure decreases the compressive strength of concrete in the DBS15F numerical model, more damaged areas are observed compared to the DBS15W model.

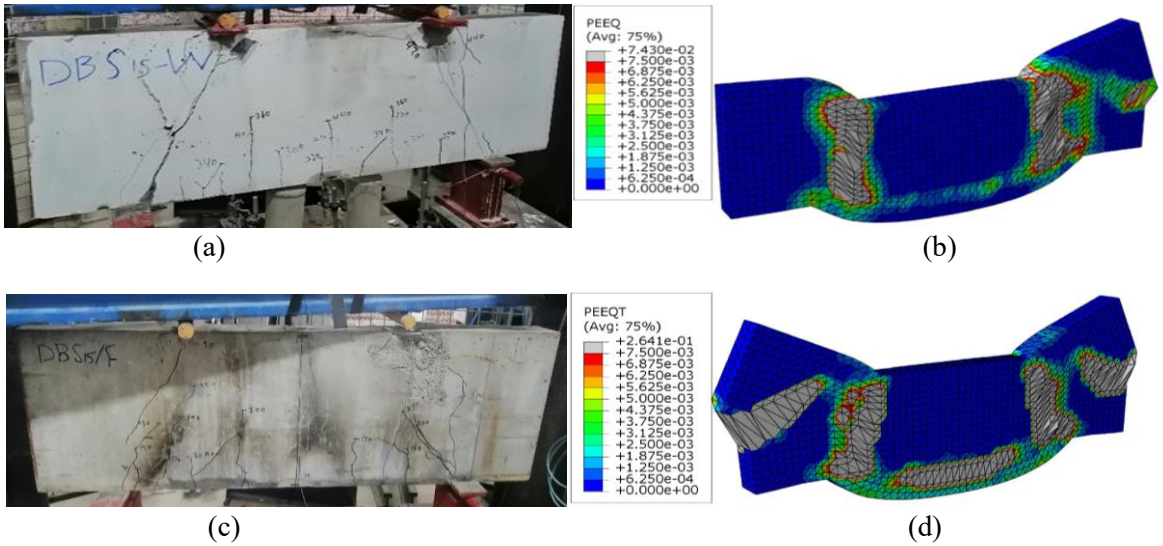


**Fig. 14.** cracking pattern for a) DBS15W experimental specimen b) DBS15W numerical model c) DBS15F experimental specimen d) DBS15F numerical model

## 4.3. Stress analysis of numerical models

A benefit of numerical modeling is the insightful understanding it provides of force transfer mechanisms and stresses in the different components of experimental specimens. The force transfer mechanism in numerical models at the final moment of loading is depicted in Figure 15, with the red color indicating tensile stress and the blue color illustrating compressive stress.

As indicated in Figure 15, a bottle-shaped strut with an arc-like path [7,49], transfers the compressive force of numerical models from the load application point to the support area. In other words, the compressive load transfer mechanism operates as a restrained arc after cracking occurs.

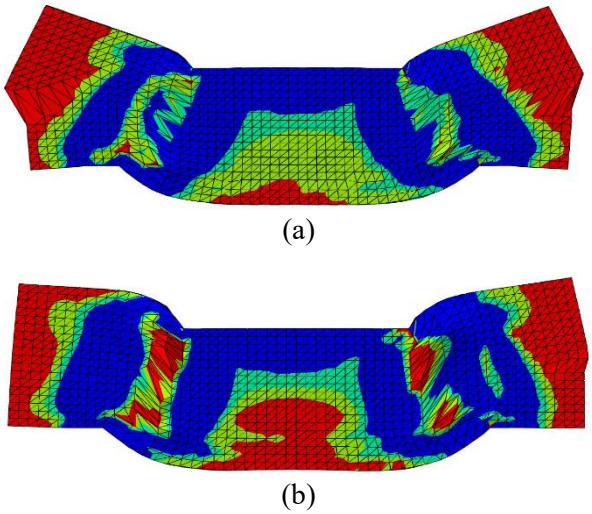


**Fig. 15.** load transfer mechanism in a) numerical model of DBS15W b) numerical model of DBS15F.

The height of the deep beam creates an arc-shaped function in the numerical models, and reducing the height of the numerical models prevents the formation of the arc-shaped mechanism. Factors such as fire conditions, confinement, distance between shear reinforcements, and the compressive strength of concrete significantly affect the compressive capacity of struts. An increase in the distance between shear reinforcements and a decrease in confinement can lower the compressive capacity of the struts, resulting in a decrease in the shear capacity of the deep beam. Fire conditions, in addition to the drop in concrete compressive strength and damage to the deep beams, can impair the compressive capacity of compression arms and deteriorate the shear capacity of deep beams. According to Figure 15, a tie region is formed in the middle and lower part of the LRCDBs in numerical models due to the applied load. In these areas, after the onset of concrete cracking, the tensile reinforcements act as ties for tensile capacity, increasing the shear capacity of deep beams.

The state of reinforcements in the samples at the moment of failure is illustrated in Figure 16. It is evident that tensile reinforcements play a crucial role in load-bearing. In the sample exposed to fire, DBS15F, fewer points in the tensile reinforcements are yielded at the moment of failure. Tensile reinforcements do not exhibit high bearing capacity until the sample fails, which could be due to the loss of concrete strength, spalling of concrete, or a decrease in the resistance of tensile reinforcements under the effect of heat. The stirrups undergo significant deformations prior to yielding, but they do not rupture.

## 5. Conclusion

1. Significant achievements are observed in the research regarding the effects of fire on concrete. It shows a 33% decrease in compressive strength, from 37.81 MPa to 25.33 MPa, and a 47% decrease in tensile strength, from 2.78 MPa to 1.48 MPa.

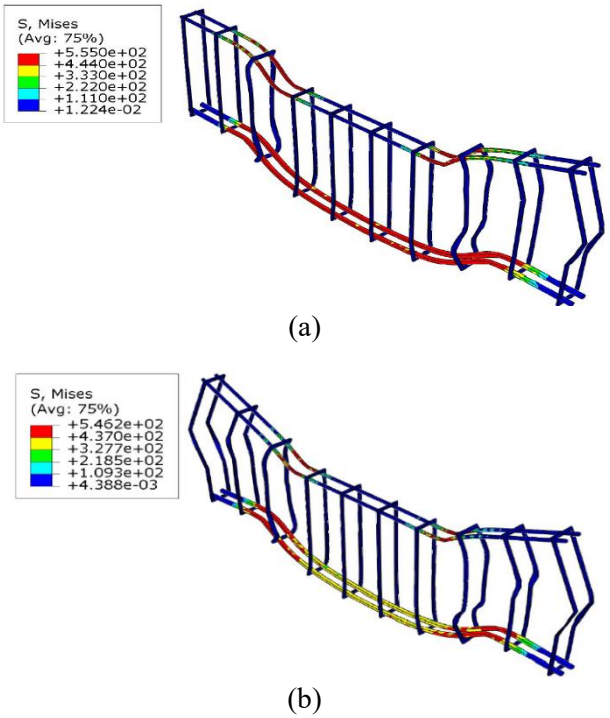


**Fig. 16.** Von Mises stress contour at the failure moment in a) numerical model of DBS15W b) numerical model of DBS15F.

2. For samples with a stirrup distance of 150 mm, the ultimate load is decreased by 23.6%, from 526.75 KN to 402.16 KN. Likewise, for samples with a stirrup distance of 60 mm, the ultimate load experiences a decrease of 16.8%, from 563.05 KN to 468.50 KN.

3. The cracking load is decreased by 53.3% and 50% for samples with stirrup distances of 150 mm and 60 mm, respectively.

4. Increasing the distance from 60 to 150 mm results in a reduction in the ultimate load from 563.05 KN to 526.75 KN before fire. After fire exposure, the ultimate load further decreases, from 468.50 KN to 402.16 KN, with increased reinforcement distance.

5. Fire causes a decrease in stiffness. It shows an 8% and 11.2% decrease in stiffness for samples with stirrup distances of 150 mm and 60 mm, respectively. The spacing of reinforcements does not significantly impact stiffness.

6. After fire exposure, the ultimate deflection decreases by 17.3% and 12.9% for samples

with stirrup distances of 150 mm and 60 mm, respectively. Additionally, reducing the stirrup spacing from 150 mm to 60 mm increases the ultimate deflection by 1.7% and 7.1% at normal temperature and after fire, respectively.

7. The study reveals a shift in the mode of failure as the distance between transverse reinforcements decreases and the samples are exposed to fire. The mode of failure shifts towards flexural failure under these conditions.

8. Numerical modeling results are successfully validated with experimental findings. The study emphasizes the logical arc path of compressive force on LRCDBs, enhancing beam shear capacity in strut-operated regions. However, it also highlights that factors such as increased distance between shear reinforcements, reduced confinement, and fire damage can decrease the compressive capacity of the struts, ultimately reducing the shear capacity of LRCDBs.

## 6. Future Studies

Future studies in this area could encompass the following:

1. More experimental tests with varied geometries and reinforcement details to validate and expand the initial findings.

2. Implementing finite element analysis for a larger number of deep beam models to simulate their behavior under fire conditions.

3. Conducting parametric studies to investigate the effects of different parameters on the beams' fire performance.

4. Developing performance-based design guidelines for lightweight reinforced concrete deep beams exposed to fire

5. comparing the result of this study with normal concrete in an experimental or modeling procedure. This comparison will likely focus on the reduced weight and increased porosity of lightweight aggregates, which can impact the interlocking of aggregates and the compressive zone concrete.

## Declaration

Ethical statements: We affirm that the manuscript consists of our own original work, devoid of any prior publication. The paper accurately and comprehensively represents our research and analysis.

## Conflicts of interest

The authors declare that there is no conflict of interest.

## References

[1] ACI Committee 318. Building code requirements for structural concrete (ACI 318-08) and commentary, American Concrete Institute; 2008.

[2] Kong FK. Reinforced concrete deep beams. CRC Press; 1991.

[3] Jin L, Lei Y, Song B, Jiang X, DU X. Meso-scale modelling of size effect on shear behavior of Basalt fiber reinforced concrete deep beams. Compos Struct 2023;304:116440. https://doi.org/10.1016/j.compstruct.2022.116440.

[4] Jin L, Lei Y, Yu W, Du X. Dynamic shear failure and size effect in BFRP-reinforced concrete deep beam. Eng Struct 2021;245:112951. https://doi.org/10.1016/j.engstruct.2021.112951.

[5] Si X-Y, Zhang G-Y, Zheng C, Xu C-Y, Xu H, Wang Y-L. Experimental study on shear behavior of reinforced concrete deep beams with high-strength bars under uniform load. Structures 2022;41:553–67. https://doi.org/10.1016/j.istruc.2022.05.018.

[6] Rogowsky DM, MacGregor JG. Design of reinforced concrete deep beams. Concr Int 1986;8:49–58.

[7] Abdul-Razzaq KS, Mustafa Jalil A, Asaad Dawood A. Reinforcing struts and ties in concrete continuous deep beams. Eng Struct 2021;240:112339.

https://doi.org/10.1016/j.engstruct.2021.112339.

[8] Mustafa TS, Beshara FBA, Abd El-Maula AS, Fathi MG. Strut-and-tie model for FRP effectiveness in shear strengthening of RC deep beams. Eur J Environ Civ Eng 2023;27:593–608. https://doi.org/10.1080/19648189.2022.2056248.

[9] Sagar Varma Sagi M, Lakavath C, Suriya Prakash S. Effect of steel fibers on the shear behavior of Self-Compacting reinforced concrete deep Beams: An experimental investigation and analytical model. Eng Struct 2022;269:114802. https://doi.org/10.1016/j.engstruct.2022.114802.

[10] Zingoni A. Current Perspectives and New Directions in Mechanics, Modelling and Design of Structural Systems. London: CRC Press; 2022. https://doi.org/10.1201/9781003348443.

[11] Youssf O, Hassanli R, Mills JE, Abd Elrahman M. An experimental investigation of the mechanical performance and structural application of LECA-Rubcrete. Constr Build Mater 2018;175:239–53. https://doi.org/10.1016/j.conbuildmat.2018.04.184.

[12] Soltanabadi R, Behfarnia K. Shear strength of reinforced concrete deep beams containing recycled concrete aggregate and recycled asphalt pavement. Constr Build Mater 2022;314:125597. https://doi.org/10.1016/j.conbuildmat.2021.125597.

[13] Albidah AS. Shear behviour of metakaolin-fly ash based geopolymer concrete deep beams. Eng Struct 2023;275:115271. https://doi.org/10.1016/j.engstruct.2022.115271.

[14] Demir A, Caglar N, Ozturk H. Parameters affecting diagonal cracking behavior of reinforced concrete deep beams. Eng Struct 2019;184:217–31. https://doi.org/10.1016/j.engstruct.2019.01.090.

[15] Kopańska A, Nagrodzka-Godycka K. The influence of reinforcement on load carrying capacity and cracking of the reinforced concrete deep beam joint. Eng Struct 2016;107:23–33. https://doi.org/10.1016/j.engstruct.2015.11.001.

[16] Liu J, Mihaylov BI. A comparative study of models for shear strength of reinforced concrete deep beams. Eng Struct 2016;112:81–9. https://doi.org/10.1016/j.engstruct.2016.01.012.

[17] Chen H, Yi W-J, Hwang H-J. Cracking strut-and-tie model for shear strength evaluation of reinforced concrete deep beams. Eng Struct 2018;163:396–408. https://doi.org/10.1016/j.engstruct.2018.02.077.

[18] Yang K-H, Ashour AF. Strut-and-Tie Model Based on Crack Band Theory for Deep Beams. J Struct Eng 2011;137:1030–8. https://doi.org/10.1061/(ASCE)ST.1943-541X.0000351.

[19] Li Y, Chen H, Yi W-J, Peng F, Li Z, Zhou Y. Effect of member depth and concrete strength on shear strength of RC deep beams without transverse reinforcement. Eng Struct 2021;241:112427. https://doi.org/10.1016/j.engstruct.2021.112427.

[20] Nassif MK, Erfan AM, Fadel OT, El-sayed TA. Flexural behavior of high strength concrete deep beams reinforced with GFRP bars. Case Stud Constr Mater 2021;15:e00613. https://doi.org/10.1016/j.cscm.2021.e00613.

[21] Yousef AM, Tahwia AM, Marami NA. Minimum shear reinforcement for ultra-high performance fiber reinforced concrete deep beams. Constr Build Mater 2018;184:177–85. https://doi.org/10.1016/j.conbuildmat.2018.06.022.

[22] Ibrahim M, Wakjira T, Ebead U. Shear strengthening of reinforced concrete deep beams using near-surface mounted hybrid carbon/glass fibre reinforced polymer strips. Eng Struct 2020;210:110412. https://doi.org/10.1016/j.engstruct.2020.110412.

[23] Peng F, Cai Y, Yi W, Xue W. Shear behavior of two-span continuous concrete deep beams reinforced with GFRP bars. Eng Struct 2023;290:116367. https://doi.org/10.1016/j.engstruct.2023.116367.

[24] Nawaz W, Elchalakani M, Yehia S, Xie T, Liu H, Yang B, et al. Shear strengthening performance of GFRP reinforced lightweight SCC beams: Experimental and

analytical study. Eng Struct 2023;278:115545. https://doi.org/10.1016/j.engstruct.2022.115545.

[25] Shaaban IG, Zaher AH, Said M, Montaser W, Ramadan M, Abd Elhameed GN. Effect of partial replacement of coarse aggregate by polystyrene balls on the shear behaviour of deep beams with web openings. Case Stud Constr Mater 2020;12:e00328. https://doi.org/10.1016/j.cscm.2019.e00328.

[26] Garcia S, Pereira A, Pierott R. Shear strength of sand-lightweight concrete deep beams with steel fibers. ACI Struct J 2021;118:203–14.

[27] Dabbaghi F, Yang TY, Tanhadoust A, Emadi SB, Dehestani M, Yousefpour H. Experimental and numerical investigation on post-fire seismic performance of light weight aggregate reinforced concrete beams. Eng Struct 2022;268:114791. https://doi.org/10.1016/j.engstruct.2022.114791.

[28] Fan S, Zhang Y, Tan KH. Fire behaviour of deep beams under unsymmetrical loading. Eng Struct 2022;250:113419. https://doi.org/10.1016/j.engstruct.2021.113419.

[29] Alqarni AS, Albidah AS, Abadel AA. Shear performance of reinforced concrete deep beams using different coarse aggregates under the effect of elevated temperatures. Case Stud Constr Mater 2022;16:e01087. https://doi.org/10.1016/j.cscm.2022.e01087.

[30] Tan KH, Lu HY. Shear behavior of large reinforced concrete deep beams and code comparisons. Struct J 1999;96:836–46.

[31] Augustino DS, Kabubo C, Kanali C, Onchiri RO. The orientation effect of opening and internal strengthening on shear performance of deep concrete beam using recycled tyre steel fibres. Results Eng 2022;15:100561. https://doi.org/10.1016/j.rineng.2022.100561.

[32] Rajesh Kumar K, Yuvanesh Kumar R. Structural behaviour of deep beam using hybrid fiber reinforced concrete with M−sand. Mater Today Proc 2022;68:1481–5. https://doi.org/10.1016/j.matpr.2022.07.097.

[33] Lin Y, Yan J, Wang Z, Fan F, Zou C. Ultimate capacity and failure mechanism of SCS and S-UHPC composite deep beams: Test and modeling. Eng Struct 2021;245:112874. https://doi.org/10.1016/j.engstruct.2021.112874.

[34] Alshannag MJ, Alshenawy AO. Enhancing the flexural performance of lightweight reinforced concrete beams exposed to elevated temperatures. Ain Shams Eng J 2021;12:2575–83. https://doi.org/10.1016/j.asej.2020.12.020.

[35] Fan S, Zhang Y, Tan KH. Experimental and analytical studies of reinforced concrete short beams at elevated temperatures. Eng Struct 2020;212:110445. https://doi.org/10.1016/j.engstruct.2020.110445.

[36] Astm C. Standard test method for sieve analysis of fine and coarse aggregates. ASTM C136-06 2006.

[37] Aggregates AICC on C and C. Standard test method for compressive strength of cylindrical concrete specimens. ASTM international; 2014.

[38] ASTM A. C496/C496M-17, Standard test method for splitting tensile strength of cylindrical concrete specimens ASTM C-496. West Conshohocken ASTM Int 2011.

[39] Duthinh D. Structural Design for Fire: A Survey of Building Codes and Standards. Gaithersburg, MD: 2014. https://doi.org/10.6028/NIST.TN.1842.

[40] Omar Z, Sugiman S, Yussof MM, Ahmad H. The effects of woven fabric Kenaf FRP plates flexural strengthened on plain concrete beam under a four-point bending test. Case Stud Constr Mater 2022;17:e01503. https://doi.org/10.1016/j.cscm.2022.e01503.

[41] Aguilar G, Matamoros AB, Parra-Montesinos G, Ramírez JA, Wight JK. Experimental evaluation of design procedures for shear strength of deep reinfoced concrete beams, American Concrete Institute; 2002.

[42] Hussein G, Sayed SH, Nasr NE, Mostafa AM. Effect of loading and supporting area on shear strength and size effect of concrete deep beams. Ain Shams Eng J 2018;9:2823–31. https://doi.org/10.1016/j.asej.2017.11.002.

[43] Oh J-K, Shin S-W. Shear strength of reinforced high-strength concrete deep beams. Struct J 2001;98:164–73.

[44] Albu-Hassan NH, Al-Thairy H. Experimental and numerical investigation on the behavior of hybrid concrete beams reinforced with GFRP bars after exposure to elevated temperature. Structures 2020;28:537–51. https://doi.org/10.1016/j.istruc.2020.08.079.

[45] Akinpelu M, Adedeji AA. Structural Response of Reinforced Self-Compacting Concrete Deep Beam Using Finite Element Method. J Soft Comput Civ Eng 2018;2:36–61. https://doi.org/10.22115/scce.2018.50115.

[46] Rehman A, Masood A, Akhtar S, Ibrahim SM, Shariq M. Experimental and numerical investigation into flexural bond strength of RC beams exposed to elevated temperature. Constr Build Mater 2021;282:122630. https://doi.org/10.1016/j.conbuildmat.2021.122630.

[47] Akhaveissy AH, Desai CS. Application of the DSC model for nonlinear analysis of reinforced concrete frames. Finite Elem Anal Des 2012;50:98–107. https://doi.org/10.1016/j.finel.2011.09.001.

[48] Zargarian M, Rahai A. Theoretical and Experimental Studies of Two-Span Reinforced Concrete Deep Beams and Comparisons with Strut-and-Tie Method. Adv Civ Eng 2021;2021. https://doi.org/10.1155/2021/8880067.

[49] Moradi M, Esfahani MR. Application of the strut-and-tie method for steel fiber reinforced concrete deep beams. Constr Build Mater 2017;131:423–37. https://doi.org/10.1016/j.conbuildmat.2016.11.042.